A Bio-Inspired Analog Silicon Retina with Michaelis-Menten Auto-Adaptive Pixels Sensitive to Small and Large Changes in Light

Stefano Mafrica, Stéphanie Godiot, Mohsine Menouni, Marc Boyron, Fabien Expert, Raphaël Juston, Nicolas Marchand, Franck Ruffier, Stéphane Viollet

A bio-inspired analog silicon retina with Michaelis-Menten auto-adaptive pixels sensitive to small and large changes in light

Stefano Mafrica,[1,2,*] **Stéphanie Godiot,**[3] **Mohsine Menouni,**[3] **Marc Boyron,**[1] **Fabien Expert,**[1] **Raphaël Juston,**[1] **Nicolas Marchand,**[4] **Franck Ruffier,**[1,*] **Stéphane Viollet**[1]

[1]*Aix-Marseille Université, CNRS, ISM UMR 7287, 13288 Marseille, France*
[2]*PSA Peugeot Citroën, Route de Gisy, 78140 Vélizy-Villacoublay, France*
[3]*Aix-Marseille Université, CNRS/IN2P3, CPPM UMR 7346, 13288 Marseille, France*
[4]*GIPSA-lab Laboratory, Control Systems Department, SySCo team, CNRS, University of Grenoble, ENSE3 BP 46, 38402 St Martin d'Hères Cedex, France*
[*]*stefano.mafrica@univ-amu.fr; franck.ruffier@univ-amu.fr*

Abstract: In this paper, we present: (i) a novel analog silicon retina featuring auto-adaptive pixels that obey the Michaelis-Menten law, i.e. $V = V_m \frac{I^n}{I^n+\sigma^n}$; (ii) a method of characterizing silicon retinas, which makes it possible to accurately assess the pixels' response to transient luminous changes in a $\pm$3-decade range, as well as changes in the initial steady-state intensity in a 7-decade range. The novel pixel, called M^{2}APix, which stands for Michaelis-Menten Auto-Adaptive Pixel, can auto-adapt in a 7-decade range and responds appropriately to step changes up to $\pm$3 decades in size without causing any saturation of the Very Large Scale Integration (VLSI) transistors. Thanks to the intrinsic properties of the Michaelis-Menten equation, the pixel output always remains within a constant limited voltage range. The range of the Analog to Digital Converter (ADC) was therefore adjusted so as to obtain a Least Significant Bit (LSB) voltage of 2.35mV and an effective resolution of about 9 bits. The results presented here show that the M^{2}APix produced a quasi-linear contrast response once it had adapted to the average luminosity. Differently to what occurs in its biological counterparts, neither the sensitivity to changes in light nor the contrast response of the M^{2}APix depend on the mean luminosity (i.e. the ambient lighting conditions). Lastly, a full comparison between the M^{2}APix and the Delbrück auto-adaptive pixel is provided.

OCIS codes: (110.1085) Adaptive imaging; (230.6046) Smart pixel systems; (230.0250) Optoelectronics; (330.7320) Vision adaptation; (330.5310) Vision - photoreceptors; (330.1800) Vision - contrast sensitivity.

References and links

1. F. Expert and F. Ruffier, "Flying over uneven moving terrain based on optic-flow cues without any need for reference frames or accelerometers," Bioinspir. Biomim. (to be published in February 2015).
2. A. Spivak, A. Belenky, A. Fish and O. Yadid-Pecht, "Wide-Dynamic-Range CMOS Image Sensors - Comparative Performance Analysis," IEEE Trans. Electron Devices **56**, 2446–2461 (2009).

3. L. Liu, J. Wiinschmann, N. P. Aryan, A. Zohny, M. Fischer, S. Kibbel, and A. Rothermel, "An ambient light adaptive subretinal stimulator," in *Proc. ESSCIRC '09* (IEEE, 2009), pp. 420–423.
4. D. Drazen, P. Lichtsteiner, P. Häfliger, T. Delbrück, and A. Jensen, "Toward real-time particle tracking using an event-based dynamic vision sensor," Exp. Fluids **51**, 1465–1469 (2011).
5. J. Carneiro, S.-H. Ieng, C. Posch, and R. Benosman, "Event-based 3D reconstruction from neuromorphic retinas," Neural Networks **45**, 27–38 (2013).
6. C. Pacoret and S. Régnier, "A review of haptic optical tweezers for an interactive microworld exploration," Rev. Sci. Instrum. **84**, 081301 (2013).
7. K. I. Naka and W. A. H. Rushton, "S-potentials from luminosity units in the retina of fish (Cyprinidae)," J. Physiol. **185**, 536–555 (1966).
8. L. Michaelis and M. L. Menten, "The Kinetics of Invertase Action (Die Kinetik der Invertinwirkung)," Biochemische Zeitschrift **49**, 333–369 (1913).
9. F. S. Werblin, "Adaptation in a vertebrate retina: intracellular recording in Necturus," J. Neurophysiol. **34**, 228–241 (1971).
10. R. A. Normann and I. Perlman, "The effects of background illumination on the photoresponses of red and green cones," J. Physiol. **286**, 491–507 (1979).
11. W. S. Geisler, "Effects of bleaching and backgrounds on the flash response of the cone system," J. Physiol. **50**, 413–434 (1981).
12. S. Laughlin and M. Weckstrom, "Fast and slow photoreceptors - a comparative study of the functional diversity of coding and conductances in the Diptera," J. Comp. Physiol., A **172**, 593–609 (1993).
13. C. A. Mead and M. Mahowald, "A silicon model of early visual processing," Neural Networks **1**, 91–97 (1988).
14. T. Delbrück and C. A. Mead, "An electronic photoreceptor sensitive to small changes in intensity," in *Adv. Neural Inf. Process. Syst. 1,* D. S. Touretzky, ed. (Morgan Kaufmann, 1989), pp. 720–727.
15. K. A. Boahen and A. G. Andreou, "A Contrast Sensitive Silicon Retina with Reciprocal Synapses," in *Adv. Neural Inf. Process. Syst. 4,* D. S. Touretzky, ed. (Morgan Kaufmann, 1991), pp. 764–772.
16. T. Delbrück and C. A. Mead, "Analog VLSI Adaptive, Logarithmic, Wide-Dynamic-Range Photoreceptor," in *IEEE Int. Symp. Circuits Syst. (ISCAS '94),* (IEEE, 1994), pp. 339–342.
17. K. A. Zaghloul and K. Boahen, "A silicon retina that reproduces signals in the optic nerve," J. Neural Eng. **3**, 257–267 (2006).
18. P. Lichtsteiner, C. Posch, and T. Delbrück, "A 128x128 120 dB 15 μs Latency Asynchronous Temporal Contrast Vision Sensor," IEEE J. Solid-State Circuits **43**, 566–576 (2008).
19. K. Shimonomura, S. Kameda, A. Iwata, and T. Yagi, "Wide-dynamic-range APS-based silicon retina with brightness constancy," IEEE Trans. Neural Networks **22**, 1482–93 (2011).
20. E. Reinhard and K. Devlin, "Dynamic range reduction inspired by photoreceptor physiology," IEEE Trans. Vis. Comput. Graphics **11**, 13–24 (2005).
21. L. Meylan, D. Alleysson, and S. Süsstrunk, "Model of retinal local adaptation for the tone mapping of color filter array images," J. Opt. Soc. Am. A **24**, 2807–2816 (2007).
22. N.-S. Vu and A. Caplier, "Illumination-robust face recognition using retina modeling," in *IEEE Int. Conf. Image Process. (ICIP '09),* (IEEE, 2009), pp. 3289–3292.
23. S. Ferradans, M. Bertalmio, E. Provenzi, and V. Caselles, "An analysis of visual adaptation and contrast perception for tone mapping," IEEE Trans. Pattern Anal. Mach. Intell. **33**, 2002–2012 (2011).
24. E. Zrenner, "Will Retinal Implants Restore Vision?," Science **295**, 1022–1025 (2002).
25. K. Stingl, K. U. Bartz-Schmidt, D. Besch, A. Braun, A. Bruckmann, F. Gekeler, U. Greppmaier, S. Hipp, G. Hörtdörfer, C. Kernstock, H. Koitschev, A. Kusnyerik, H. Sachs, A. Schatz, K. T. Stingl, T. Peters, B. Wilhelm, and E. Zrenner, "Artificial vision with wirelessly powered subretinal electronic implant alpha-IMS," Proc. R. Soc. London, Ser. B **280**, (2013).
26. F. S. Werblin, "Control of Retinal Sensitivity II: Lateral Interactions at the Outer Plexiform Layer," J. Gen. Physiol. **63**, 62–87 (1974).
27. T. Delbrück, "Investigations of visual transduction and motion processing," Ph.D. thesis, California Inst. Tech., Pasadena, California (1993).
28. F. Expert, S. Viollet, and F. Ruffier, "Outdoor field performances of insect-based visual motion sensors," J. Field Robot. **28**, 529–541 (2012).
29. G. Sicard, H. Abbas, H. Amhaz, H. Zimouche, R. Rolland, and D. Alleysson, "A CMOS HDR Imager with an Analog Local Adaptation," in *Int. Image Sensor Workshop (IISW '13),* (2013), pp. 1–4.
30. D. A. Baylor and M. G. F. Fuortes, "Electrical responses of single cones in the retina of the turtle," J. Physiol. **207**, 77–92 (1970).
31. R. M. Boynton and D. N. Whitten, "Visual Adaptation in Monkey Cones: Recordings of Late Receptor Potentials," Science **170**, 1423–1426 (1970).
32. J. Kleinschmidt and J. E. Dowling, "Intracellular Recordings from Gecko Photoreceptors during Light and Dark Adaptation," J. Gen. Physiol. **66**, 617–648 (1975).
33. D. C. Hood and P. A. Hock, "Light adaptation of the receptors: Increment threshold functions for the frog's rods and cones," Vision Res. **15**, 545–553 (1975).

34. S. B. Laughlin and R. C. Hardie, "Common strategies for light adaptation in the peripheral visual systems of fly and dragonfly," J. Comp. Physiol., A **128**, 319–340 (1978).
35. G. Svaetichin, "The cone action potential," Acta Physiol. **29**, 565–600 (1953).
36. T. Oikawa, T. Ogawa, and K. Motokawa, "Origin of so-called cone action potential," J. Neurophysiol. **22**, 102–111 (1959).
37. J. M. Valeton, "Photoreceptor light adaptation models: an evaluation," Vision Res. **23**, 1549–1554 (1983).
38. D. Floreano, R. Pericet-Camara, S. Viollet, F. Ruffier, A. Brückner, R. Leitel, W. Buss, M. Menouni, F. Expert, R. Juston, M. K. Dobrzynski, G. L'Eplattenier, F. Recktenwald, H. a. Mallot, and N. Franceschini, "Miniature curved artificial compound eyes," Proc. Nat. Acad. Sci. U. S. A. **110**, 9267–72 (2013).
39. S. Viollet, S. Godiot, R. Leitel, W. Buss, P. Breugnon, M. Menouni, R. Juston, F. Expert, F. Colonnier, G. L'Eplattenier, A. BrÃŒckner, F. Kraze, H. Mallot, N. Franceschini, R. Pericet-Camara, F. Ruffier, and D. Floreano D., "Hardware Architecture and Cutting-Edge Assembly Process of a Tiny Curved Compound Eye," Sensors **110**, 21702–21721 (2014).
40. S.-C. Liu, J. Kramer, G. Indiveri, T. Delbrück, and R. Douglas, *Analog VLSI: Circuits and Principles* (MIT Press, 2002).
41. P. Venier and X. Arreguit, "Réseau de cellules photosensibles et capteur d'images comportant un tel réseau," French Patent, Patent No.: EP0792063A1 (1997).
42. G. Sabiron, P. Chavent, T. Raharijaona, P. Fabiani, and F. Ruffier, "Low-speed optic-flow sensor onboard an unmanned helicopter flying outside over fields," in *IEEE Int. Conf. Robot. Autom. (ICRA '13),* (IEEE, 2013), pp. 1742–1749.

1. Introduction

During the last few decades, research in the field of robotics has advanced considerably, but there still exist very few sighted robots which are able to behave appropriately, regardless of changes in the illuminance (see Fig. 5 in [1], for instance), such as those which occur outdoors. One of the reasons for this lack is that it is difficult to design pixels that combine high sensitivity with a wide luminosity range.

A large variety of Wide-Dynamic-Range (WDR) CMOS image sensors has been proposed throughout the years [2], trying to widen the operating luminosity range as much as the visible spectrum while keeping sensitivity to small changes for every average luminosity in the operating range. Although the WDR image sensors capture images in a luminosity range of up to 7 decades, they provide different contrast sensitivities at different average luminosities. Vision applications such as event-based and bio-medical applications often require high and constant sensitivity in a large luminosity range, in order to detect small temporal and/or spatial changes in the intensity in several lighting conditions [3–6]. One possible solution to this problem can be found by looking at the auto-adaptive response of human and animal photoreceptors.

In their physiological studies on fish, Naka and Rushton established for the first time that a vertebrate retina obeys a process of adaptation whereby each photoreceptor's response is normalized by a representative value of the average local luminosity [7], in line with the Michaelis-Menten equation [8]. In the light of these and subsequent findings [7, 9–12], many efforts have been made to mimic the Outer Plexiform Layer (OPL) circuitry in silicon retinas [3, 13–19], or to implement the model in software for image processing [20–23]. In the latter case, the normalization giving the adaptation is implemented numerically after digitalization which gives rise to noise amplification, especially in dark scenes. Consequently, considerable interest has focused during the last twenty years on developing a silicon retina giving an OPL-like response over the entire visible spectrum, also thanks to the latest advances in retinal implant systems [24, 25].

The first example of an auto-adaptive silicon retina was presented in [13], where a logarithmic photoreceptor was used to handle transient changes in light in a 1-decade range, while light adaptation within a 1-decade range was obtained by "subtracting" a local spatio-temporal average. This circuit improved the contrast resolution of equally illuminated areas in comparison with standard logarithmic photoreceptor retinas, but there was no improvement in the low signal-to-noise ratio inherent to the logarithmic amplification. In [14], a modified version of this chip was compared with the OPL response described in *Necturus* [26] (see Section 2), showing

light adaptation in a 5-decade range but sensitivity to luminous changes within a range of only 0.5 decades.

To overcome these limitations, a more biologically inspired solution was subsequently developed in a study by [15], which consisted in modulating the synaptic strengths locally to control the sensitivity and including cone-to-cone gap junctions to attenuate the noise. Although the sensitivity was improved in this way from 0.5 to 2 decades, the adaptation to light was not satisfactory because of the circuit deviations resulting from the increasing inter-receptor coupling strength. A good compromise between contrast sensitivity and light adaptation was reached in [16], which gave light adaptation in a 6-decade range and sensitivity in a 1-decade range. However, the steady-state response of this pixel was found to increase with the light intensity (i.e., the photodiode current) and the transient response was not always monotonic when large lighting variations occurred (see Fig. 2.13 in [27]). The Delbrück adaptive pixel was also found in studies on optic flow measurements to have little practical use in situations where changes in the light greater than 1 decade are liable to occur (see Figs. 7(b),7(d),7(j) and 7(l) from [28]). In [29], the Gamma correction method presented in [21] for local tone-mapping purposes was improved by digitally normalizing the pixel output directly in VLSI in line with the Michaelis-Menten law: only a few preliminary results on light adaptation and contrast sensitivity were presented, however, in that study.

Other solutions not involving the use of auto-adaptive elements have been suggested. In [3], a subretinal stimulator was endowed with light adaptation by shifting the dynamic input range via an externally generated signal. The results presented showed that photoreceptor adaptation was achieved in a 7-decade range. In [19], a silicon retina was provided with a wide dynamic operating range and a high contrast sensitivity by applying a spatial and temporal filtering process based on resistive networks. The results obtained showed that the pixels could deal with 4 decades of luminosity changes, but their contrast responses depended on the external voltage controlling a reset transistor.

As far as we know, no artificial retinas have ever been endowed up to now with pixels with the following features at once: (i) auto-adaptation to the mean local luminosity over a range as wide as the visible spectrum; (ii) constant sensitivity to luminous changes, i.e. contrasts, at any average luminosity in the operating range; (iii) reliable response even in the presence of sudden large changes in the luminosity (i.e., without causing circuit saturations or deviations).

In this paper, it is proposed to present: (i) a novel analog silicon retina featuring auto-adaptive pixels that obey the Michaelis-Menten law faithfully in a 7-decade range without causing any saturation of the VLSI transistors, while keeping an effective resolution of the integrated analog-to-digital conversion of about 9 bits; (ii) a method of characterizing silicon retinas, which can be used to accurately assess the pixels' response to transient luminous changes within a $\pm$3-decade range and to changes in the steady-state intensity within a 7-decade range. We have called this novel pixel the M^2APix, which stands for the Michaelis-Menten Auto-adaptive Pixel.

The present artificial retina consists of a $2 \times 2\,mm$ CMOS circuit comprising four lines of six auto-adaptive pixels, and a digital interface giving a fast serial read-out of up to $1\,MHz$ connecting the retina directly to an external microprocessor or microcontroller. The adaptation time constant of the M^2APix can be changed by means of an external capacitor, providing additional flexibility to eventually meet the application's requirements in term of preferred bandwidth.

The biological background to this study is presented in Section 2. The chip implementation is presented in Section 3, and a detailed description of our auto-adaptive pixel is provided in Section 4. The method of characterization used is presented in Section 5, and the results obtained using this method are presented and discussed in Section 6. A comparison between the M^2APix and the Delbrück pixel present on the same silicon retina is proposed in Section 7.

Some conclusions are reached in the last section.

2. Biological background

Light adaptation of the photoreceptors present in human and animal retinas has been extensively studied in a large number of species since the early 50's, using both intra and extracellular methods [7, 9, 11, 30–34]. In all these studies, the relationship between light stimuli and photoreceptor responses has been documented, both in the dark and with background illumination, via an adaptation process described by the so-called Michaelis-Menten equation [8]:

$$V = V_m \frac{I^n}{I^n + \sigma^n}, \tag{1}$$

where V stands for the photoreceptor's response and V_m is its maximum value; I denotes the light intensity and n usually ranges from 0.7 to 1; σ is the adaptation parameter, corresponding to the light intensity giving half of the maximum response.

The first micro-electrode recordings of rod and cone responses were obtained on saltwater fish (*Gerridae*) by Svaetichin in 1953 [35]. In his pioneering study, Svaetichin discovered the S-potentials, as they were subsequently called by Oikawa *et al.* in [36], which stands for "slow potentials", referring to the slow adaptation process which occurs in the photoreceptor potentials when they are exposed to flash lights against a steady background.

However, the first mathematical description of the cone response given by equation (1) was provided by Naka and Rushton in the case of the freshwater fish (*Cyprinidae*) [7]. The equation (1) where $n = 1$ is therefore also known as the Naka-Rushton law. The same model was subsequently validated and applied to turtles' cones by Baylor *et al.* [30] and to monkeys' cones by Boynton and Whitten [31], who introduced the exponent $n < 1$ for the first time. Many studies were then carried out on vertebrates and invertebrates, all confirming the equation in (1) with various values of n and sometimes with different interpretations of the adaptation parameter σ (in the salamander [9], gecko [32], frog [33], locust, fly and dragonfly [34], for instance, and in the human fovea [11]).

Figure 1 shows the responses of dark- and light-adapted red cone photoreceptors recorded intracellularly in the retina of the turtle (*Pseduemys Scripta Elegans*) by Normann and Perlman [10]. As can be seen from this figure, the function $V(I)$ defined in (1) gives rise in the $Log(I)$ domain to curves with a fairly smooth "S" shape (continuous curves), where the slope of the "S" is given by the value of n ($n = 1$ in that case) and the lateral shift by the value of σ.

Based on the S-shaped curves shown in Fig. 1, two main features of the light-adaptation behavior can be described by the incident-light model [37]:

- as the background lighting changes, the entire S-shaped curve shifts along the light intensity axis, which corresponds to a change in the sensitivity of the photoreceptor in the neighborhood of the background light. In fact, after reaching a peak value caused by an increase/decrease in the intensity of the light (data points), the potential V gradually returns to a steady-state value, reflecting its adaptation to the background. This decrease/increase in V corresponds to a "slow" increase/decrease in the parameter σ (see equation (1));

- as the background illumination increases, the operating point of the photoreceptor increases correspondingly (small horizontal lines in Fig. 1), which means that because of the non-linearity of the curve, the response to a given increment/decrement in the stimulus becomes smaller/larger at higher background levels. This process known as "response compression" was introduced for the first time by Boynton and Whitten in [31]. The slope of the curve around the operating point defines the contrast sensitivity.

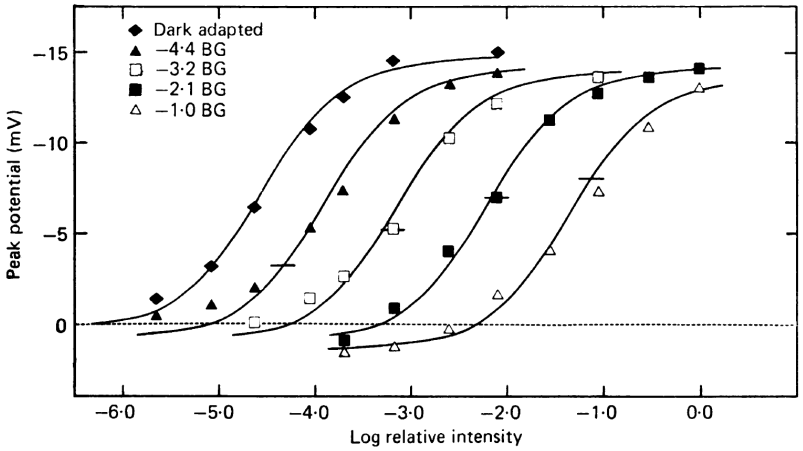

Fig. 1. S-shaped curves corresponding to dark- and light-adapted response curves recorded in a red cone of the turtle. The peak of either the incremental or decremental response measured from the dark-adapted potential recorded before the background onset (dashed line) is plotted as a function of the log of the test pulse intensity which elicited each response. The steady hyperpolarization produced by each background lighting condition is given by the intersection between the intensity-response curve and the small horizontal line. The continuous curves were drawn from a single template which describes the function $V = V_m \frac{I}{I+\sigma}$. Adapted from [10].

3. Chip implementation

In this section, we present our 2-D photosensor array, featuring a silicon retina composed of 24 auto-adaptive pixels of two different kinds. A picture of the chip package, with a zoom on the retina, is presented in Fig. 2.

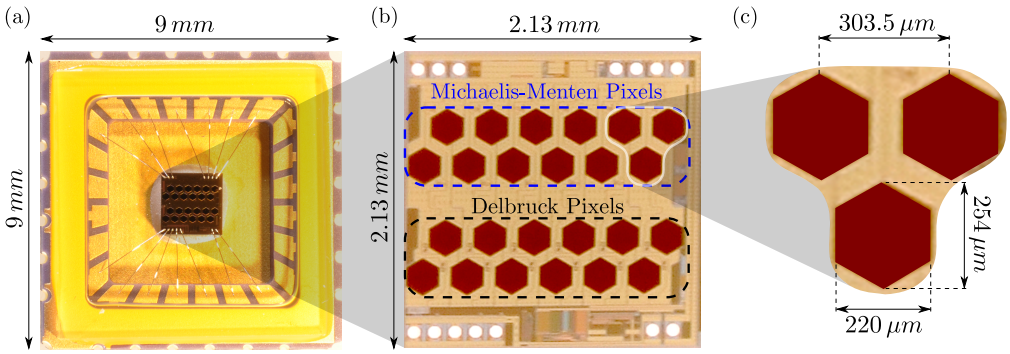

Fig. 2. (a) The silicon retina in its $9 \times 9mm$ package; (b) Magnified view of the silicon retina composed of 12 Michaelis-Menten pixels presented in this study, and 12 additional Delbrück pixels; (c) Magnified view of 3 Michaelis-Menten pixels giving the photodiode's dimensions and the inter-receptor distance.

The retina consists of a $2 \times 2mm$ CMOS circuit designed using the $350nm$ XFAB standard CMOS process. To facilitate the integration of the chip into custom-made Printed Circuit Boards (PCBs), the circuit was encapsulated in a standard $9 \times 9mm$ (LCC24) package with 24 pins. Four rows of auto-adaptive pixels with a $254\,\mu m$ diameter N-well/P-substrate photodiode

were implemented in the PCB, as shown in Fig. 2(a). The photodiode is mostly sensitive to red light ($\lambda \approx 650nm$) and its sensitivity S_{ph} is equal to $1.1 \times 10^{-8} \frac{Am^2}{W}$. The retina is completely self-biased and can be read out by means of digital serial read-out architecture implemented directly on the chip. The main functional blocks implemented on the chip can therefore be summarized as follows:

- two rows of six Michaelis-Menten auto-adaptive pixels, that we called M^{2}APix (see Section 4 for details);
- a low-pass filtered current-averaging cell and the reference voltage, required by the Michaelis-Menten architecture (see Section 4);
- a bias generator providing the polarization currents required for the circuit to operate properly;
- a reference voltage for the analog-to-digital converter (ADC);
- a digital serial interface, which includes the digitizing of the pixel output signals via a 10-bit ADC, and a direct serial communication bus (see details below).

In addition, two rows of six pixels of the Delbrück type (see [16] for more details) were implemented on the same chip.

The photodiodes were aligned on two horizontally staggered rows so that the hexagons fit together like a puzzle, recalling the shape and the arrangement of insects' hexagonal ommatidia (Fig. 2). This pattern of alignment of the photodiodes, which is particularly suitable for detecting luminous contrasts in the main direction, also makes it possible to sense light variations in any other direction.

The analog signals originating from each pixel were digitized on-chip so that they could be directly processed by an external microprocessor or microcontroller, saving the power consumption and the computational resources of the latter for further data processing. Since the pixel type is selected by a digital input, only one set of pixels can be converted at a time. The twelve M^{2}APix outputs are low-pass filtered with a cut-off frequency of $300Hz$ before being digitally converted, giving a minimum sampling frequency of $600Hz$ in order to prevent the occurrence of aliasing. An integrated DC reference voltage was connected to the ADC as an additional pixel output for testing and calibration purposes. To improve the LSB voltage, the dynamic input range of the ADC can be reduced by using an external voltage source. A synchronous direct-connection protocol similar to that used in the artificial compound eye CurvACE [38] was adopted, as it provides a very simple, robust solution.

A functional diagram of the interface protocol is given in Fig. 3. For the serial communications, a similar internal state machine working with a maximum frequency of $1MHz$ to that adopted in the CurvACE sensor [38] was used to transfer the data to an external device.

4. M^{2}APix: Michaelis-Menten auto-adaptive pixel

In this section, we present our novel auto-adaptive pixel implementing the Michaelis-Menten model in analog VLSI, as described in Section 2. The theoretical basis of the analog circuit is first presented, and an example of the auto-adaptive pixel's response is then given to illustrate the behavior of the M^{2}APix and show how the pixel is related to S-shaped curves such as those presented in Fig. 1.

4.1. Circuit description

The block scheme depicted in Fig. 4(a) gives an overview of the Michaelis-Menten pixel implementation. All the blocks in the area delimited by the dashed lines belong to a single pixel.

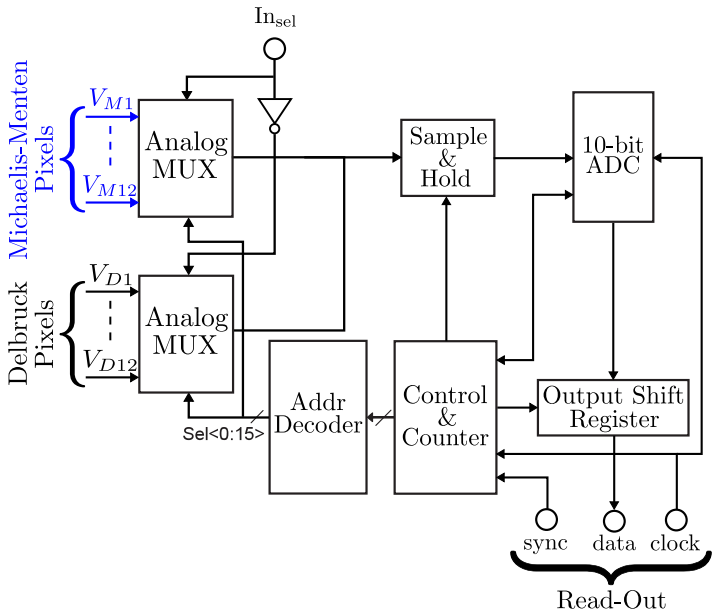

Fig. 3. Block diagram of the retina's serial synchronous read-out interface (see [39]).

These blocks are therefore replicated twelve times, whereas the two blocks outside the dashed-line area are common to all twelve pixels.

To implement the Michaelis-Menten function in (1), we adopted the current normalizer model presented in [40] (Chapter 6, pp. 148-150), with an arbitrary number of current inputs, and patented in [41] in the context of photosensing. In the present application, two current inputs are required: one for the photodiode current I_{ph_i} and one for the current I_{0_i} corresponding to the average illuminance. The functional scheme of the current normalizer is presented in Fig. 4(b). A switch S can be used to select either I_{0_i} as the mean current I_{mean_i} provided by the built-in averaging circuit or an external current I_{ext_i} provided by an external circuit. In what follows, we take $I_{0_i} = I_{mean_i}$.

The scheme adopted here improves the functioning of the current normalizer by adjusting the V_{ref} voltage to a different value from that of V_{dd} ($3.3\,V$). The auto-adaptive pixels we designed work efficiently in a wide range of luminosities corresponding to a photodiode current ranging from about $20\,pA$ to $20\,\mu A$. The V_{ref} voltage optimizes the functioning of the system at low currents by preventing the current source M_b transistor from saturating.

Operating principle of the normalizer

If the transistors $M_1, \ldots, M_4$ have the same dimensions and are working in their sub-threshold region, the current output I_{out_i} can be expressed as follows:

$$I_{out_i} = I_b \frac{I_{ph_i}}{I_{ph_i} + I_{mean_i}}, \tag{2}$$

where $I_b = 50\,nA$ and the index $i = 1 \ldots 12$ gives the number of pixels. For the sake of simplicity, we will drop the index in what follows.

To obtain the same auto-adaptation to light as that which occurs in animals' eyes, I_{mean} has to be a representative value of the background luminosity perceived by the artificial retina (see

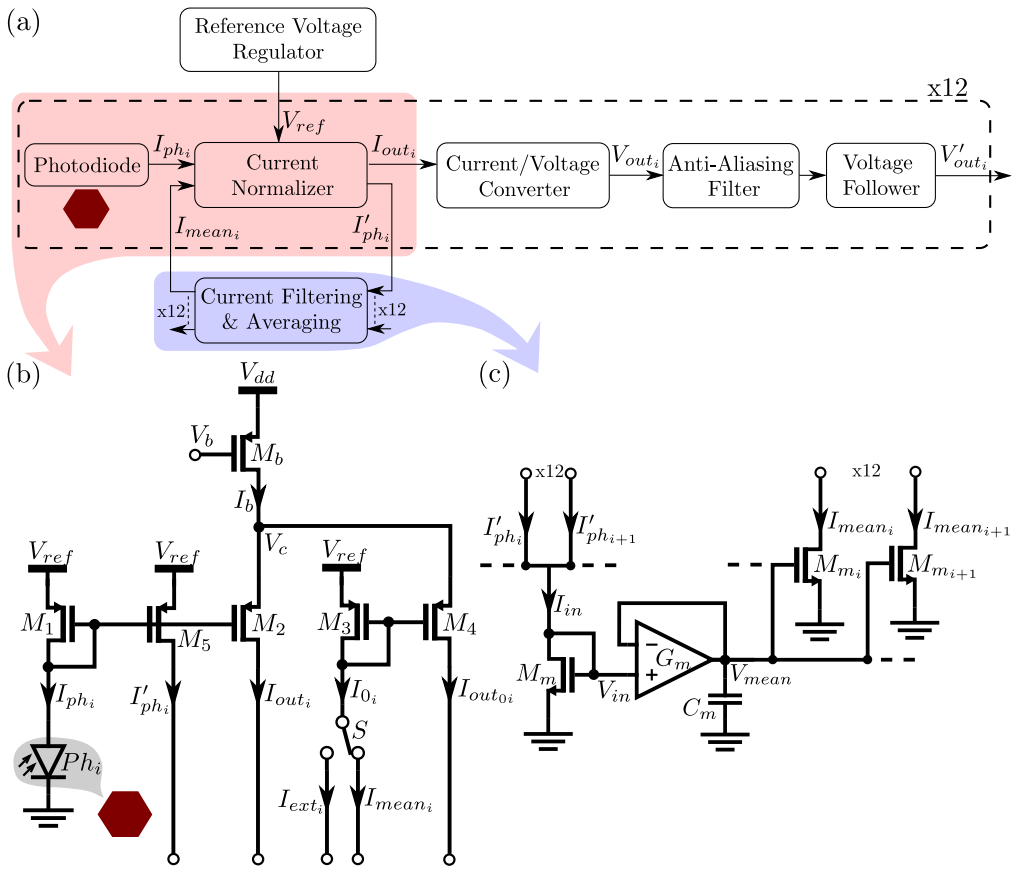

Fig. 4. (a) Block diagram of the M^{2}APix: Michaelis-Menten Auto-adaptive Pixel. The blocks in the dashed-line area, which are replicated 12 times, belong to a single pixel, whereas the two blocks outside the dashed-line area are common to all twelve pixels. (b) Hardware implementation in VLSI of an elementary auto-adaptive pixel (photodiode and current normalizer), the output signal of which is noted I_{out_i}. A switch S can be used to select either I_{0_i} as the mean current I_{mean_i} provided by the built-in averaging circuit, or an external current I_{ext_i} provided by an external circuit. (c) Hardware implementation in VLSI of the filtering and averaging circuit computing the mean current of the 12 mirrored photodiode currents (I'_{ph_i}) produced by the 12 normalizer circuits.

Section 1 and 2). Accordingly, the computation of I_{mean} must reflect only the low-frequency changes in the light perceived by all the photoreceptors in the retina. The current I_{mean} is therefore the average value of copies of all 12 photodiode currents (I'_{ph_i}) filtered with a first order low-pass filter. As shown in Fig. 4(c), the low-pass filter is provided by a gm-C structure using an operational transconductance amplifier (OTA) G_m and an external capacitor C_m. In particular, if the external capacity is set at $100\,nF$, as done in our tests, the cut-off frequency will be $150\,mHz$.

As shown in Fig. 4(a), the output current of the normalizer is converted into a voltage via a high gain transimpedance amplifier (TIA). This high-factor current-to-voltage conversion R_f is obtained using a low-transconductance OTA in the feedback loop of an operational amplifier stage. The output voltage V_{out} can therefore be expressed as follows:

$$V_{out} = -R_f I_{out}, \tag{3}$$

where R_f is set at $17.5\,M\Omega$ via the OTA transconductance.

To prevent the occurrence of aliasing due to the sampling frequency of the digital conversion, a first-order low-pass filter with a gm-C structure is added to each pixel. A cut-off frequency of $300\,Hz$ is achieved by means of a low-transconductance OTA and an internal capacitance.

Lastly, a voltage follower helps the pixel to drive the input sampling capacitance of the ADC.

The output pixel voltage can then be written as follows:

$$V_{out} = -R_f I_b \frac{I_{ph}}{I_{ph} + I_{mean}} + V_{BG}, \tag{4}$$

where $V_{BG} \approx 2.3\,V$ denotes the band-gap voltage due to the intrinsic functioning of the various stages.

4.2. M²APix response

The fact that the term I_{mean} in equation (4) corresponds to the average luminosity constitutes a key point in the adaptive behavior of the pixel.

Let us assume that in the absence of any optical lenses placed on the retina, all the pixels are exposed to the same light intensity. If no changes or only very slow changes in the luminosity occur, all the photodiode currents and their average will be identical. Therefore by substituting $I_{mean} = I_{ph}$ into (4), the steady-state value of the pixel's output can be obtained:

$$V_{out_0} = -\frac{R_f I_b}{2} + V_{BG}, \tag{5}$$

which is a constant value depending only on the operating current I_b and not on the photodiode currents.

This feature is the main difference with respect to the biological findings, which on the contrary, show the existence of a logarithmic increase in the steady-state response with respect to the luminosity, giving rise to the so called "response compression" (see Section 2). In fact, while the contrast sensitivity of the OPL varies, depending on the average luminosity (see for instance the slope around the small horizontal line of the full-triangle curve in comparison with the empty-triangle one in Fig. 1), our silicon retina shows the same contrast sensitivity whatever the average luminosity. In other words, an object showing a contrast of 10% will generate the same signal amplitude at the output of the M^2APix under both low and high luminosity levels.

In order to explain this behavior more clearly and show how it is related to S-shaped curves such as those presented in Fig. 1, an example of the pixel's response was plotted as shown in Fig. 5(a).

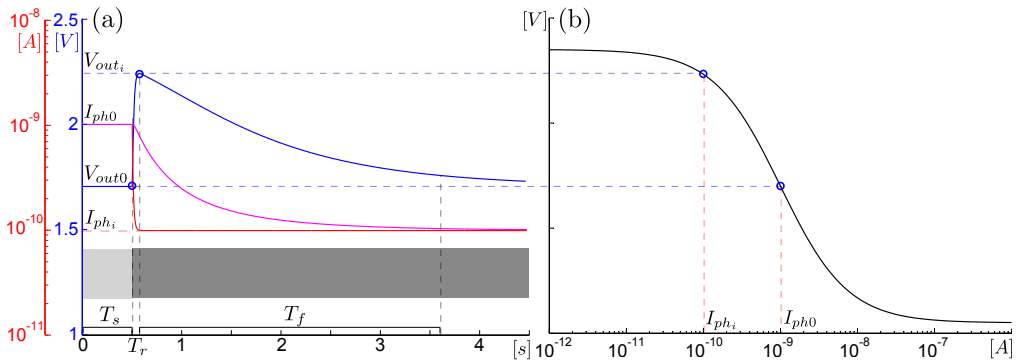

Fig. 5. (a) Simulated example of the adaptive pixel's response (blue line) to a step change in the light intensity (light to dark gray stripe). The red and magenta lines stand for the photodiode current and the average current, respectively. (b) Theoretical S-shaped curve based on equation (4), giving the peak values of the pixel's response V_i to step changes in the photodiode current from I_{ph_0} to I_{ph_i}.

At the time t_0, all the photodiode currents and the pixel's output are stabilized at I_{ph_0} and V_{out_0}, respectively. Then, after the time T_s, a step change in the luminosity occurs in front of the silicon retina, making all the photodiode currents "rapidly" change from I_{ph_0} to I_{ph_i} (red line), while the average current changes much more slowly (magenta line). During the stabilization of the average current, the pixel's output first increases from V_{out_0} to the peak value V_{out_i}, and then decreases until it reaches its stable baseline value V_{out_0} (blue line) again. We take *rise time* (T_r) to denote the time taken by V_{out} to go from V_{out_0} to 90% of $(V_{out_i} - V_{out_0})$ and *fall time* (T_f) the time taken by the signal to go from V_{out_i} to 90% of $(V_{out_0} - V_{out_i})$. It can be shown that T_r and T_f mainly depend on the photodiode and transistors time-constant and the averaging block time-constant ($\tau_m = \frac{C_m}{G_m}$), respectively.

As $T_r \ll \tau_m$, it can be assumed that when $V_{out} = V_{out_i}$, I_{mean} does not change ($I_{mean} \approx I_{ph_0}$) independently from I_{ph_i}. Therefore, the points defining the S-shaped curve correspond to the peak values V_{out_i} reached at all the step values I_{ph_i} after the same initial value I_{ph_0} (Fig. 5(b)). It is worth noting that when the value of I_{ph_i} reaches up to ± 1 decades of I_{ph_0}, the pixel shows a logarithmic sensitivity to changes in the lighting conditions (see the sloping part of the curve around the operating point), while the sensitivity decreases drastically in response to greater changes in the light.

Thanks to the intrinsic properties of the normalization, the peak values depend only on the ratio $\frac{I_{ph_i}}{I_{ph_0}}$, resulting in a horizontal shift of the S-shaped curve depending on I_{ph_i} in the same way as the curves in Fig. 1.

In addition, as I_{ph} is linearly proportional to the luminous intensity, we can assume the presence of a luminous contrast defined by the Michelson formula: $c_i = \frac{I_{ph_i} - I_{ph_0}}{I_{ph_i} + I_{ph_0}}$. Substituting the inverse of this formula into equation (4), i.e. $I_{ph_i} = \frac{1+c_i}{1-c_i} I_{ph_0}$, we obtain:

$$V_{out_i} = -R_f I_b \frac{c_i + 1}{2} + V_{BG}. \tag{6}$$

The pixel can therefore be said to give a linear contrast response, and the contrast resolution is given by the coefficient of c_i in equation (6).

Lastly, an AC noise simulation was performed with a white noise at the input (corresponding to the shot noise of the photodiode), to obtain the Root Mean Square (RMS) of the output

noise and consequently the minimum detectable contrast for different values of the average luminosity, i.e. the DC photodiode current. The RMS values are given by integrating the output noise in $[10^{-5}, 10^{8}]\,Hz$. The minimum detectable contrast can be defined as the contrast that gives rise to a transient response of the output signal $\pm$6-fold the RMS noise.

Figure 6 shows the RMS of the simulated output noise (blue) and the minimum detectable contrast (red) with respect to the photodiode current. We can notice that the noise is decreasing with the DC photodiode current. At very low background luminosity, the noise is dominated by the input white noise of the photodiode which is amplified by the gain of the circuit. At higher luminosity, this gain is smaller, so the simulated input noise becomes negligible and the output noise is nearly equal to the transistors' noise. In any case, the RMS values obtained are always very low compared to the output variations $(V_{out_i} - V_{out_0})$ in the transient response, as shown in the simulated response in Fig. 5. Consequently, the minimum detectable contrast is very low over the entire operating range of the average luminosity, varying from $\pm 1.1\,\%$ at $1\,Lux$ to $\pm 0.4\,\%$ at $10^5\,Lux$.

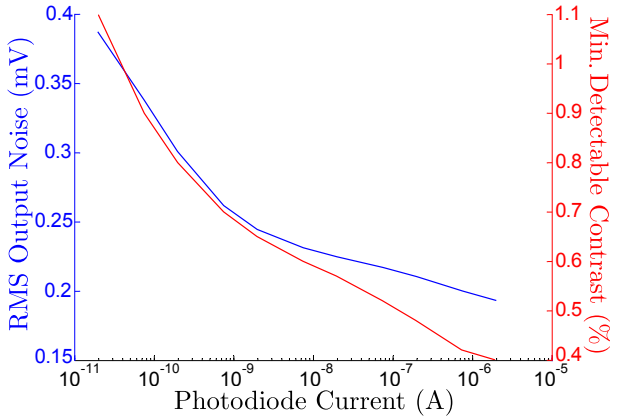

Fig. 6. Root Mean Square (RMS) of the simulated output noise (blue) and corresponding minimum detectable contrast (red) with respect to the photodiode current. The RMS values are given by integrating in $[10^{-5}, 10^{8}]\,Hz$ the output noise obtained with an AC noise simulation which takes into account all the transistor noises and a white noise for the input photodiode. The minimum detectable contrast can be defined as the contrast that gives rise to a transient response of the output signal $\pm$6-fold the RMS noise.

5. Method of characterization

In the studies presented in Section 1, the light adaptation and contrast sensitivity of silicon retinas were often tested by applying a series of lighting steps (AC light) in addition to various background lights (DC light). As a result, the pixels' responses have often been described in terms of the stimulus intensity, and direct comparisons can therefore be made with the biological findings (see Section 2). However, the method used to characterize pixels' responses is sometimes not clear or has not even been described at all, which makes comparisons with other results very difficult.

A standard method is presented here for accurately characterizing pixels' responses to luminous changes of up to ± 3 decades in a 7-decade mean luminosity range by implementing a single light source, which has been called the *Lighting Box* (Fig. 7).

The Lighting Box consists of a $50 \times 25 \times 25\,mm$ 3-D printed box with a $10 \times 10\,mm$ aperture. The Lighting Box also includes a Printed Circuit Board (PCB) which accurately controls the

light intensity of a red Light Emitting Diode (LED) (TLWR7600, Vishay Semiconductors) by means of a specific digital current driver (ADN8810, Analog Devices). The PCB with the LED and the PCB supporting the retina to be characterized are fixed to each side of the box so that both the LED and the silicon retina can fit into the aperture, facing each other inside the box (see Fig. 7(b)). The box also contains an optical filter support, which can be inserted between the LED and the retina in order to attenuate the LED's intensity and thus characterize the pixel's response in the illuminance range of interest.

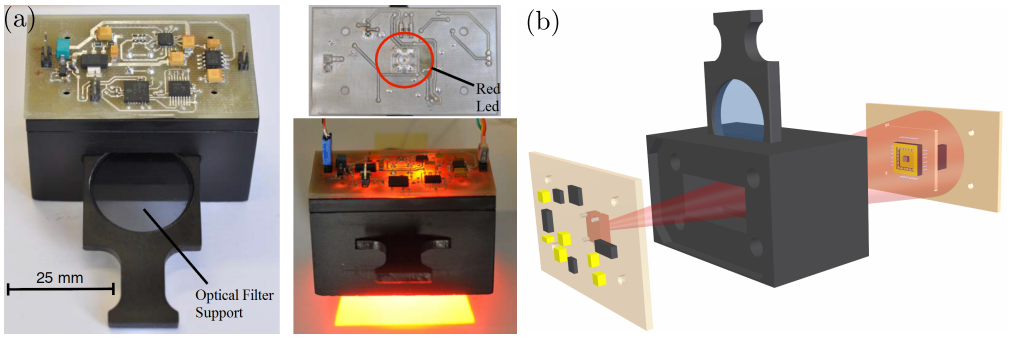

Fig. 7. (a) Pictures and (b) exploded view of the *Lighting Box* composed of a PCB with a red LED ($\lambda \approx 618\,nm$) and an optical filter support. The direct control of the LED current makes the illuminance vary in a 3-decade range. Additional optical filters (neutral density filters) were used to drastically increase the mean luminosity range from 3 to 7 decades.

The following main tools were used for this purpose:

- The Lighting Box described above.
- A NI Single-Board RIO-9683 Acquisition Device provided by National Instruments. The board features a $400\,MHz$ real-time processor with 128 MB DRAM and includes an integrated real-time controller and a 2-Million-Gate reconfigurable FPGA programmed using LabVIEW software including Real-Time and FPGA modules.
- An Explorer 16 development board provided by Microchip, which includes a dsPIC 33FJ128GP804 micro-controller working at a sampling rate of $2\,kHz$. This device was programmed using Matlab/Simulink with a toolbox specifically developed for use with Microchip dsPIC micro-controllers.

The block diagram in Fig. 8 gives an overview of the hardware setup and communication flow involved in the method of characterization.

Characterization procedure

The 12 pixels' output signals were acquired while they were being exposed to step changes in the luminous intensity, as described in Section 4.2. During the overall acquisition process, the FPGA acts as the master component handling and synchronizing the communications with the Lighting Box in order to drive the intensity of the LED, and with the Explorer 16 in order to acquire data from the chip. Based on Fig. 5 and Fig. 8, the i-th step in the procedure can be described as follows:

1. The FPGA sends the Lighting Box a packet of four bytes (Led Data) containing the information about the initial value (I_{LED_0}) and the step value (I_{LED_i}) of the LED intensity.

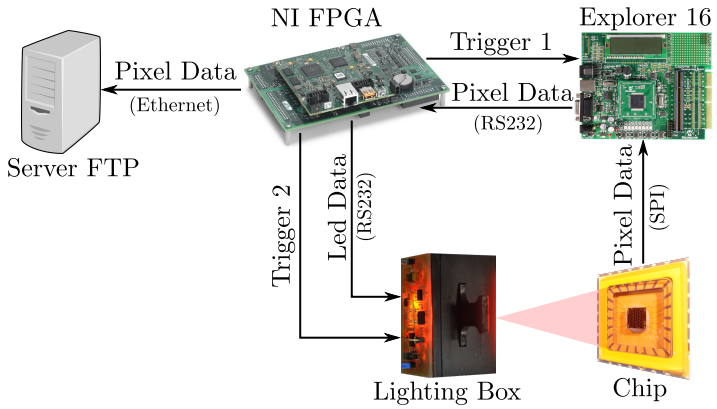

Fig. 8. Block diagram of the hardware setup and communication flow involved in the pixel characterization procedure.

2. As soon as the Lighting Box receives the packet, it sets the LED intensity at the initial value I_{LED_0}.

3. After waiting for a time (T_{wait}), which is usually the time required for the pixel output to reach its steady-state value, the FPGA sends Explorer 16 a trigger signal (Trigger 1) making it start sending the data acquired. The steady-state value of the pixels is thus acquired before the lighting change occurs.

4. A short instant later (T_s), the FPGA sends the Lighting Box a second trigger signal (Trigger 2) making it switch the LED intensity from I_{LED_0} to I_{LED_i} (see Fig. 5).

5. The Explorer 16 sends the FPGA the appropriate number of samples (Pixel Data), depending on the sampling frequency.

6. The FPGA stores the data acquired in a FTP server and goes back to step 1 to deal with the next pair I_{LED_0}, I_{LED_i}.

The current-irradiance characteristic of the LED was assessed by measuring the LED's irradiance with a radiometer (ILT1700, International Light Technologies). To obtain a good idea of what the photodiodes perceive, the radiometer was placed in front of the LED at the same distance as the chip. Therefore, without any loss of generality, I_{LED} can be taken to stand for the LED's irradiance instead of the LED current. Since the photodiode current is linearly proportional to the irradiance via the sensitivity S_{ph}, as defined in Section 3, equation (4) does not have to be changed even if we take V_{out} to be a function of I_{LED}.

As we were interested in characterizing our auto-adaptive pixel in 7 decades of photodiode current (see Section 4.1) using a LED covering three decades, four neutral optical filters (NG filters, Schott) were used: the 1 and 2 mm NG3 type for dealing with 1- and 2-decade attenuation, respectively, and the 2 and 3 mm NG9 type for dealing with 3- and 4-decade attenuation, respectively. To check the full set of S-shaped curves within ± 3 decades about I_{ph_0} (see Fig. 5(b), for example), a complete pixel characterization was carried out by merging the data obtained with the various optical filters. In particular, as the latter give contiguous 1-decade attenuation, S-shaped curves were obtained by merging and averaging the peak values V_{out_i} acquired at the same initial irradiance with several filters. For instance, the S-shaped curve centered in $0.1\,\frac{W}{m^2}$ (Fig. 5(b)) was obtained by merging the peak values obtained with $I_{LED_0} = 0.1\,mA$ without any

filter, $I_{LED_0} = 1\,mA$ with a 1-decade attenuation filter, $I_{LED_0} = 10\,mA$ with a 2-decade attenuation filter and $I_{LED_0} = 100\,mA$ with a 3-decade attenuation filter.

6. M^{2}APix characterization results

In this section, it is proposed to present and discuss the experimental data obtained when our auto-adaptive silicon retina was exposed to changes in the light, as described in Section 5.

To characterize the pixel's response in the light-adapted condition, the LED light changes were triggered when the pixel's output signal reached its steady-state value. In other words, by referring to the steps in the characterization procedure presented in Section 5, the waiting time T_{wait} in Step 3 was equal to $5T_f$, where T_f denotes the fall time, as described in Section 4.2.

6.1. M^{2}APix transient response

As mentioned in Section 4.2, we were interested in measuring the peak values V_{out_i} of the twelve pixels with each pair of photodiode currents I_{ph_0}, I_{ph_i} corresponding to a step change in the light intensity (Fig. 5). Pixel output signals were recorded with various pairs of LED irradiance values I_{LED_0}, I_{LED_i} in the $[10^{-5}, 10^2]\,\frac{W}{m^2}$ range at a sampling frequency $f_s = 2\,kHz$, in order to accurately determine the instant at which the peak value occurred, using the method described in Section 5. The set of all the mean values obtained when $I_{LED_i} = I_{LED_0}$ corresponds to the steady-state response of the pixel and constitutes an important auto-adaptive characteristic of the M^{2}APix, which will be discussed below.

Some examples of the pixel's response with $I_{LED_0} = 1\,\frac{W}{m^2}$ are presented in Fig. 9.

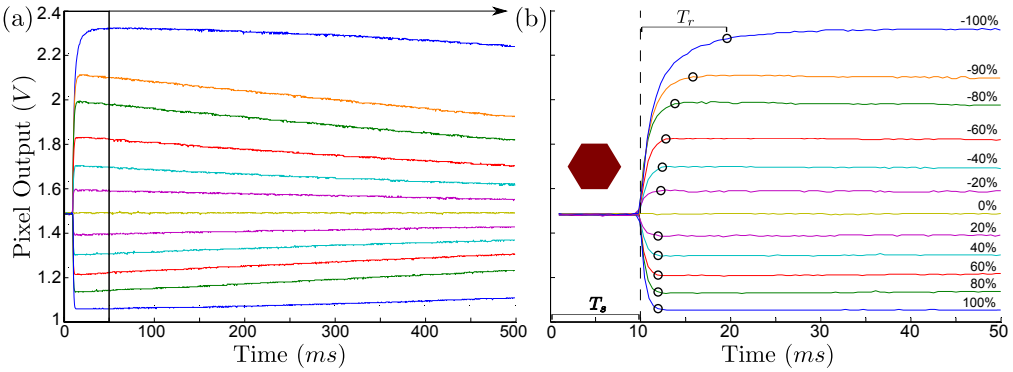

Fig. 9. (a) Example of M^{2}APix responses to step changes in the LED irradiance (I_{LED_i}), starting with the same initial irradiance $(I_{LED_0} = 1\,\frac{W}{m^2})$. (b) Zoom of the temporal pixel responses shown in Fig. 9(a) ranging between 0 and $50\,ms$. To be able to distinguish more clearly between the steady-state responses and the transient responses, the step changes were delayed by $10\,ms$ (T_s) after the acquisition procedure had started. The black circles amount to 90% of the peak values V_{out_i} and give qualitative information about the rise time (T_r). The contrast values are given by the Michelson formula $c_i = \frac{I_{LED_i} - I_{LED_0}}{I_{LED_i} + I_{LED_0}}$.

Figure 9 shows the auto-adaptation of the pixel's time response. According to the simulated example presented in Section 4.2, the pixel's output rapidly increases from the steady value V_{out_0} to a peak value V_{out_i} and then returns slowly to the steady value regardless of the contrast, which was obtained here by making step changes of I_{LED_i}. However, as shown in Fig. 9(b), the rise time (T_r), namely the time required to reach 90% of the peak value (black circles), is nearly constant with positive contrasts $(I_{LED_i} > I_{LED_0})$, but depends on the contrast with negative ones $(I_{LED_i} < I_{LED_0})$.

Figure 10 shows the mean rise time over the 12 pixels plotted with respect to the contrast. Each point corresponds to the time (T_r) required to reach 90% of the peak value V_{out_i}, as depicted in Fig. 9(b), for every step change (I_{LED_0}, I_{LED_i}).

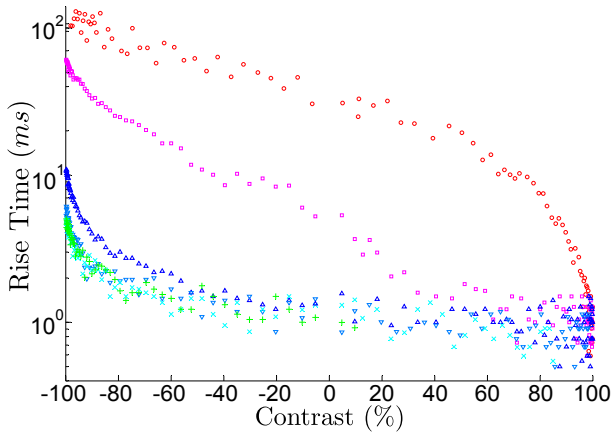

Fig. 10. Average rise time with respect to luminous contrast. Each point corresponds to the time (T_r) required to reach 90% of the peak value V_{out_i}, as depicted in Fig. 9(b). Each color refers to a different initial irradiance value I_{LED_0}: red about 0.001 $\frac{W}{m^2}$, pink about 0.01 $\frac{W}{m^2}$, dark blue about 0.1 $\frac{W}{m^2}$, light blue about 1 $\frac{W}{m^2}$, cyan about 10 $\frac{W}{m^2}$, green about 100 $\frac{W}{m^2}$.

By looking at Fig. 10, we can notice that the rise time depends on both the contrast and the average luminosity. This coupling between contrast and rise time is directly due to the current-mode functioning of the system. A high negative contrast corresponds to a normalizer's output current tending to zero, as we can see by considering $I_{ph_i} \ll I_{mean_i}$ in equation (2). The time constants of the output transistors will therefore be higher and the output signal will be slower in this case. Furthermore, the time constant of the photodiode and the transistors increases for low current, i.e. low average luminosity, explaining the higher rise times for the pink and red data points. It is worth noting that the mean rise time for positive contrasts at medium/high average luminosity (blue and green data points) is about $1\,ms$ because of the anti-aliasing low-pass filter ($F_c = 300\,Hz$, see Section 4.1).

The rise time (T_r) and the fall time (T_f) depends on the bandwidth of the output signal that is determined mainly by the photodiode and transistors time constant and the current-averaging block time constant (τ_m). Such a bandwidth can be modified by modifying the external capacitor C_m, since $\tau_m = \frac{C_m}{G_m}$ (see Section 4.1). As the fall time T_f determines the time the pixel's output takes to reach the maximum of its contrast sensitivity, i.e. the sensitivity at steady-state, it might be useful to set T_f as small as possible. If we consider an irradiance higher than $0.1\,\frac{W}{m^2}$ (about 100 Lux), the fall time T_f can be reasonably reduced up to $0.1\,s$ by changing the value of the external capacitor C_m to $5\,nF$, because the rise time T_r is lower than $0.01\,s$ for any contrast in this irradiance range. In fact, T_f should be about one decade greater than T_r to guarantee the correct functioning of the pixel in this luminosity range.

6.2. M²APix S-shaped and steady-state response

The peak values obtained in response to step changes (I_{LED_i}) starting with several initial irradiances (I_{LED_0}) are presented in Fig. 11, with respect to (a) the LED irradiance and (b) the Michelson contrast c_i, defined as follows $c_i = \frac{I_{LED_i} - I_{LED_0}}{I_{LED_i} + I_{LED_0}}$.

By comparing the S-shaped curves in Fig. 11(a) with those in Fig. 1, it can be seen in the

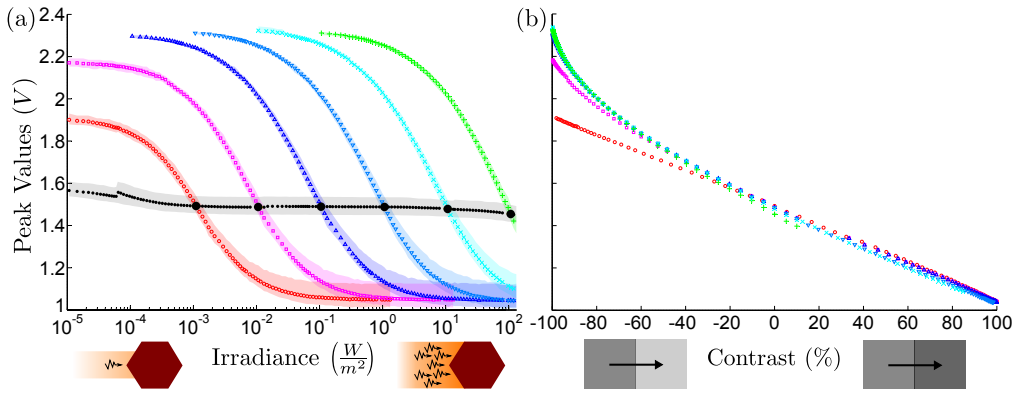

Fig. 11. (a) S-shaped curves and steady-state responses of the 12 pixels to LED irradiance changes in a 7-decade range. Each color refers to a different initial irradiance value I_{LED_0} (red about 0.001 $\frac{W}{m^2}$, pink about 0.01 $\frac{W}{m^2}$, dark blue about 0.1 $\frac{W}{m^2}$, light blue about 1 $\frac{W}{m^2}$, cyan about 10 $\frac{W}{m^2}$, green about 100 $\frac{W}{m^2}$, same color and marker as Fig. 10), and the data points correspond to the average peak value V_{out_i} reached by the 12 pixels in response to a step change in the irradiance I_{LED_i}, as shown in Fig. 5. The steady-state response (black points) was obtained with $I_{LED_i} = I_{LED_0}$ at several values of I_{LED_0}, whereas the initial values of the irradiance I_{LED_0} are indicated by large black circles. The shaded areas were obtained by plotting the minimum to maximum values of the mean pixel output voltages. The average dispersion of each curve (σ_{mean}) ranged from $37.2\,mV$ in the case of the green one, to $85.4\,mV$, in that of the red one. (b) Average peak response of the 12 pixels versus the contrast. The various curves correspond to the S-shaped curves in Fig. 11(a) (same colors and markers). The contrast is given by the Michelson formula: $c_i = \frac{I_{LED_i} - I_{LED_0}}{I_{LED_i} + I_{LED_0}}$.

first place that our silicon retina shows in qualitative terms the same adaptation process as that observed in the OPL. In particular, the pixels auto-adapt to the average light in a 7-decade range while keeping a sensitivity of nearly 600 $\frac{mV}{Log(I)}$ in a range of about 2 decades (corresponding to the linear part of the curves on the log scale). Each S-shaped curve obtained was well defined within a range of 6 decades, which means that the circuit did not deviate, but remained consistent with the model, even when the light changed suddenly by anything up to ± 3 decades, which would correspond, for instance, to shifting from a very dark overcast sky to direct sunlight (see the lower half of the dark-blue curve). In addition, in line with equation (5), the steady-state response (black points) was almost constant throughout the 7 decades, giving the same contrast sensitivity whatever the average luminosity. Lastly, upon setting the high reference of the ADC at $2.4\,V$ (see Section 3 for further details about the integrated ADC), we obtained a LSB voltage of $V_{LSB} = \frac{2.4}{2^{10}} = 2.35\,mV$, which corresponds to half of the voltage we would have obtained by setting the high reference of the ADC at V_{dd}. As the pixel output signal was limited to $[1, 2.4]\,V$, we obtained a effective resolution of the analog-to-digital conversion of $\frac{1.4\,V}{2.35\,mV} = 596 = 2^{9.22}$, i.e. about 9 bits.

The fact that the left part of the pink and red S-shaped curves is lower than that of the other ones was due to the dark current of the photodiodes. The photodiode current can be divided into 2 components: the background current I_{lbg}, which depends on the irradiance, and the dark current I_{dark}, which has a low constant value that does not depend on the irradiance. Therefore, as long as $I_{lbg} \gg I_{dark}$, we can assume that $I_{ph} \approx I_{lgb}$ and equation (4) still holds if we substitute I_{LED} into I_{ph}, whereas when $I_{lbg} \ll I_{dark}$, we have $I_{ph} \approx I_{dark}$, and V_{out} takes a constant value regardless of I_{LED}.

In addition, the dispersion of the S-shaped curves from one pixel to another can be seen in the shaded areas in Fig. 11(a). It is worth noting that this dispersion seems to be higher in the case of positive contrasts. This pattern is mainly due to the generation of the current I_b and not to the pixels themselves. As I_b is entirely conveyed to the normalizer's output current I_{out} in the case of positive contrasts, its dispersion is directly transmitted as well. This behavior can be improved by improving the dispersion of the I_b generation cell.

In Fig. 11(b), the data points in Fig. 11(a) have been plotted versus the contrast. It can be seen from this figure that the pixel's response decreased almost linearly with the luminous contrast regardless of the average luminosity, as predicted by equation (6). The non-linearity observed with highly negative contrasts was due to the non-linearity of the VLSI current-to-voltage converter. The contrast resolution K_c can be defined as the coefficient of c_i in (6) divided by 100, i.e. $K_c = -\frac{R_f I_b}{2\times 100} = -4.4\,\frac{mV}{\%}$. As the noise level is about $5\,mV$ (i.e. $2\times$LSB), contrasts as low as 2% can be detected. In addition, as the LSB voltage V_{LSB} is about 2.35mV, it is worth noting that a 1% contrast gave rise to a 2-bit change.

6.3. Faithfulness of the M²APix characterization to the Michaelis-Menten model

The absolute value of the errors observed between the peak values V_{out_i} in Fig. 11(a) and the theoretical values $V^*_{out_i}$, based on the model for the circuit defined in Section 4.1, is presented in Fig. 12. As post-layout simulations of the circuit showed that the current-to-voltage converter gave a non-linear response at low current values, the theoretical values $V^*_{out_i}$ were computed by applying a look-up table of the current-to-voltage converter to equation (2), with $I_{ph} = I_{LED}$ instead of using equation (4).

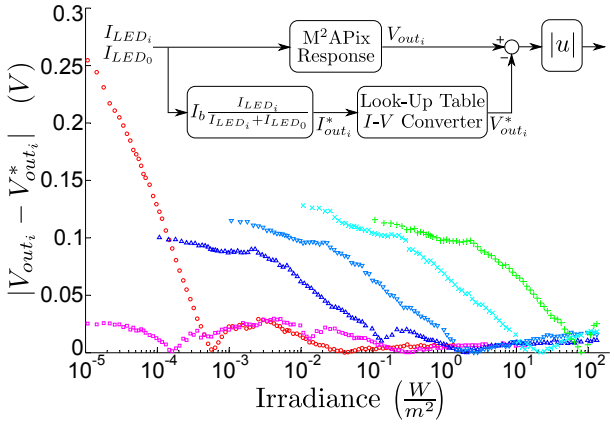

Fig. 12. Absolute value of the error between the M²APix responses measured and those predicted by the model with respect to the LED irradiance. As post-layout simulations of the circuit showed that the current-to-voltage converter gave a non-linear response at low current values, the theoretical values $V^*_{out_i}$ were computed by applying a look-up table of the current-to-voltage converter to (2), with $I_{ph} = I_{LED}$ instead of using equation (4). (Same color and marker as previous figures)

It can be noted that on each S-shaped curve (each of which is presented in a different color), the difference between the pixel output signals and the model outputs ranges from 0.1% to 8% of the whole output range, showing a good match with the Michaelis-Menten function. Possibly due to the existence of a mismatch between the actual response of the current-to-voltage converter and the simulated post-layout response, the error decreased almost monotonically with the irradiance. In addition, the existence of a greater error in the case of the red curve

($I_{LED_0} = 0.001 \frac{W}{m^2}$) was due to the presence of the photodiode dark current (I_{dark}), as explained above.

7. Comparison between M^{2}APix and Delbrück pixels

In this section, it is proposed to present a quantitative comparison between the M^{2}APix and the Delbrück pixel [16] implemented in the same silicon retina (see Fig. 2) when tested under the same conditions.

Table 1 lists all the values discussed in Section 6 for the M^{2}APix and the corresponding values obtained for the Delbrück pixel.

Table 1. Specifications of the M^{2}APix and Delbrück pixels. The main advantage is that M^{2}APix responds monotonically over very wide illuminance range without any loss of sensitivity and contrast resolution.

	M^{2}APix	Delbrück Pixel
Adaptation Range	7 decades	7 decades
Sensitivity Range	2 decades	1 decade
Sensitivity ($\pm$0.5 decade)	$600 \frac{mV}{Log(I)}$	$600 \frac{mV}{Log(I)}$
Absolute Contrast Resolution ($\pm$0.5 decade)	$4.4 \frac{mV}{\%}$	$5 \frac{mV}{\%}$
Effective Output Range ($\pm$1.5 decades)	$1.4\,V$	$0.8\,V$
DC Output Variation (7 decades)	$0.1\,V$	$0.6\,V$
Average Rise Time ($I_{LED_0} > 10^{-1} \frac{W}{m^2}$)	$\sim 1\,ms$	$\sim 1\,ms$
Maximum Rise Time ($I_{LED_0} = 10^{-3} \frac{W}{m^2}$)	$\sim 100\,ms$	$\sim 30\,ms$
Monotonic Response ($\pm$3 decades)	Yes	No
Adjustment of the Adaptation Time Constant	Yes	No

The Delbrück pixel reproduced non-monotonic responses with respect to the LED intensity for medium-high luminosity, showing unreliable responses for changes higher than ± 1 decade at $I_{LED_0} > 1 \frac{W}{m^2}$. Furthermore, the steady-state response increased with the luminosity, resulting in a higher DC output variation and a lower effective output range. Finally, the adaptation time constant of the M^{2}APix, which determines the bandwidth of the output signal, can be potentially modified externally.

To show how the two types of pixel respond to small contrasts while they are still adapting to the average luminosity, we applied the procedure presented in Section 5, but contrary to the static case (see Section 6), they were exposed to repeated sequences of $0.5\,s$-long changes in the LED irradiance (corresponding to contrasts ranging from -10 to $10\,\%$) while the average irradiance was increased by 1 or 2 decades every $5\,s$.

Figure 13 shows the time responses of one M^{2}APix and one Delbrück pixel when exposed to two different step sequences. Both types of pixel responded quickly to small changes (small contrasts) while adapting to the average luminosity, regardless of the average luminosity and the changes in the luminosity (amounting to 1 or 2 decades in this example). However, the two pixels' responses presented some remarkable differences:

- The M^{2}APix (Fig. 13(b)) consistently responded to any change in the light up to ± 2 decades, while the Delbrück pixel (Fig. 13(c)) responded asymmetrically for positive and negative changes (see the blue line in the dotted circled area at $10\,s$) and nearly did not respond to a -2-decade change (see the red line in the dotted circled area at $15\,s$).
- The M^{2}APix always reached the same steady-state value V_{out_0} independently to the average luminosity, while the Delbrück pixel reached different steady-state values for differ-

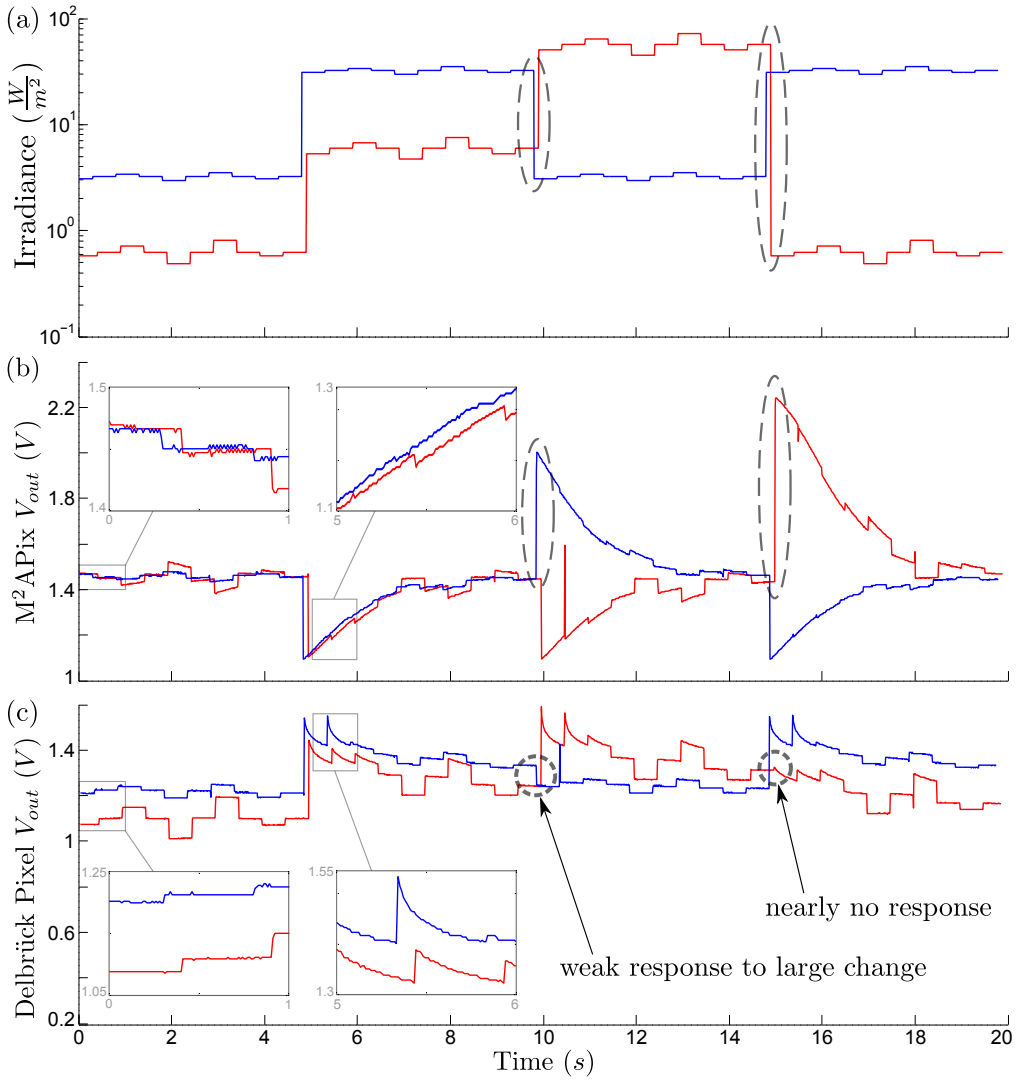

Fig. 13. (a) Two sequences of small contrasts in a 2-decade irradiance range. Time responses of (b) M^{2}APix and (c) Delbrück pixel [16], implemented in the same silicon retina (see Fig. 2), when exposed to the irradiance sequences in Fig. 13(a). The sequences were obtained by repeating: $\pm 2\%$ and $\pm 4\%$ contrasts (blue line), $\pm 6\%$ and $\pm 12\%$ contrasts (red line). The steps in the sequence were triggered every $0.5\,s$ and the changes in the average irradiance every $5\,s$. For the sake of clarity, the timing of the sequence has been slightly shifted. (The spurious peaks, such as that which occurred at 10.5 s, may have been due to some error in the data transmission)

ent average luminosity.

- The contrast response produced was not the same under both light-adapted and light-adapting conditions: it depended on the change in the light. For both types of pixel, even very small contrasts (e.g. a 2% contrast) were accurately detected when the pixel had adapted to the average luminosity (see the blue line in the left-hand zoomed part of Figs. 13(b) and 13(c)). Conversely, when adapting to a sudden large change in the light, the M^{2}APix failed to detect the same 2% contrast (see the blue line in the right-hand zoomed part of Fig. 13(b)) due to the logarithmic compression imposed by the Michaelis-Menten function and the high fall time (T_f). During this fall time (T_f), the contrast sensitivity of the pixel increases as the slope around the operating point increases when moving from V_{out_i} to V_{out_0} (see the blue circles in Fig. 5). In the same condition, the Delbrück pixel shows a very different response: the first of the two consecutive 2% contrasts is detected with a much higher gain than in the light-adapted condition while the second one is nearly not detected (see the blue line in the right-hand zoomed part of Fig. 13(c)).

It is worth noting that the M^{2}APix responded appropriately to a 6% contrast just after a 1-decade change (see the red line in the right-hand zoomed part of Fig. 13(b)), which still corresponds to a good contrast sensitivity under light-adapting conditions. Moreover, such contrast sensitivity can be improved by decreasing the time constant of the current averaging block by reducing the value of the external capacitor C_m (see Section 4.1 for details). In this way, the fall time T_f would be lower and the pixel's sensitivity would increase faster (see Section 4.2 for details).

8. Conclusion

The results presented here show that our Michaelis-Menten analog auto-adaptive pixel (called M^{2}APix) can adapt automatically to any irradiance from 10^{-5} to $10^2 \frac{W}{m^2}$, which would correspond, if the LED light was green, to an illuminance of about 7×10^{-3} and $7 \times 10^4 Lux$ respectively, that is from half moon on a clear night to nearly direct sunlight. At the same time, the results obtained showed that the circuit does not deviate from the model, even when the light suddenly changes by up to ± 3 decades, which would correspond, for instance, to shifting from a very dark overcast sky to direct sunlight.

In short, our auto-adaptive pixel can be said to have the following noteworthy features:

- adaptation to light in a 7-decade range, while remaining sensitive to changes in the light of up to about 2 decades;
- quasi-constant steady-state response in a 7-decade range: it produces the same contrast response whatever the average luminosity;
- no circuit deviations from the model within a ± 3-decade range of the operating current;
- constant limited-range responses at any average luminosity, resulting in a lower LSB voltage and therefore in a higher contrast resolution;
- minimum detectable contrast of 2% in the light-adapted condition and 6% in the light-adapting condition.

Some further improvements could be made in a future version of the M^{2}APix in the conversion stage, by subtracting $1V$ from the pixel output signal before the conversion or increasing the resistance R_f of the current-to-voltage converter in order to eventually increase the conversion range to $[0, 2.4]V$. This would increase the contrast resolution nearly two-fold, giving a

4-bit change in response to a 1% contrast, corresponding to a minimum detectable contrast of 1% in the light-adapted condition and 3% in the light-adapting condition.

Since the M^2APix makes a satisfying compromise between a high sensitivity and a wide dynamic range, it should provide a useful tool for motion detection and optical flow processing in a very large range of lighting conditions, from half-moonlight to full daylight. Thus, our auto-adaptive silicon retina, or retinas composed of larger arrays of M^2APix, could be employed in several fields, from event-based applications to bio-robotics and bio-medical applications.

In the future, we plan to test our silicon retina outdoors with a suitable optical lens both at night and in the daytime, by using it to measure the optic flow, for instance. In particular, we are willing to mount one or more M^2APix-based sensors onboard mobile and aerial robots (as in [42]) as aids to navigation under various luminosity conditions, as well as on vehicles in the case of automotive applications.

Acknowledgments

We thank the referees for their fruitful comments. We are most grateful to R. Potheau, A. Calzas and P. Breugnon for their expertise in VLSI designing and testing, to R. Leitel for the packaging and to J. Diperi for his involvement in the mechanical design. We thank F. Roubieu, A. Manecy, F. Colonnier, and R. Goulard for their helpful suggestions and comments during this study, A. Servel and S. Allano for their assistance and J. Blanc for correcting and improving the English manuscript. This research was supported partly by the CNRS (Life Science; Information and Engineering Science and Technology), Aix-Marseille University, the French National Research Agency -ANR- (EVA project under ANR-ContInt grant number ANR-08-CORD-007-04 and IRIS project under ANR-INS grant number ANR-12-INSE-0009). This research was also funded by a PhD grant from ANRT (*Association Nationale de la Recherche et de la Technologie*) as well as by PSA Peugeot Citroën via the OpenLab agreement with Aix-Marseille University and CNRS entitled “Automotive Motion Lab”.